Biochemistry

pubs.acs.org/biochemistry Article

RNA–Ligand Interactions Quantified by Surface Plasmon Resonance with Reference Subtraction

J. Winston Arney and Kevin M. Weeks*

Cite This: *Biochemistry* 2022, 61, 1625–1632 Read Online

ACCESS | Metrics & More | Article Recommendations | Supporting Information

ABSTRACT: Structured RNAs bind ligands and are attractive targets for small-molecule drugs. A wide variety of analytical methods have been used to characterize RNA–ligand interactions, but our experience is that most have significant limitations in terms of material requirements and applicability to complex RNAs. Surface plasmon resonance (SPR) potentially overcomes these limitations, but we find that the standard experimental framework measures notable nonspecific electrostatic-mediated interactions, frustrating analysis of weak RNA binders. SPR measurements are typically quantified relative to a non-target reference channel. Here, we show that referencing to a channel containing a non-binding control RNA enables subtraction of nonspecific binding contributions, allowing measurements of accurate and specific binding affinities. We validated this approach for small-molecule binders of two riboswitch RNAs with affinities ranging from nanomolar to millimolar, including low-molecular-mass fragment ligands. SPR implemented with reference subtraction reliably discriminates specific from nonspecific binding, uses RNA and ligand material efficiently, and enables rapid exploration of the ligand-binding landscape for RNA targets.

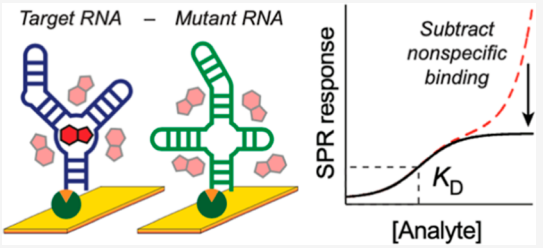

INTRODUCTION

RNA molecules have a pervasive ability to bind small molecules, extending from natural ligands that bind riboswitches[1] and the ribosome,[2] to ligands that bind artificially selected aptamers,[3,4] to potential small-molecule therapeutics.[5,6] Established methods for measuring RNA–small-molecule binding include in-line probing,[7,8] chemical probing,[9−12] electrophoretic mobility shift assays,[13] circular dichroism,[14] fluorescence of 2-aminopurine-substituted RNA,[15,16] fluorescent indicator displacement,[17] nuclear magnetic resonance,[18,19] microscale thermophoresis,[20] equilibrium dialysis,[21] size exclusion filtration,[22] isothermal titration calorimetry (ITC),[23,24] and surface plasmon resonance (SPR).[25,26]

In our own laboratory, and through conversations with colleagues in the field, we find that many strategies used to monitor RNA–small-molecule interactions have notable weaknesses. In particular, while the approaches outlined above can perform well in individual cases, we find that the above methods (i) require that large ligand-induced structural changes occur in the RNA, (ii) fail or have significant challenges when applied to complex RNAs, longer than simple or irregularly paired helices, or (iii) require large quantities of RNAs and ligands.

For larger RNAs with complex structures, our laboratory has found that two analytical methods are consistently promising: ITC and SPR. ITC enables label-free and direct thermodynamic measurements of ligand–macromolecule binding[27] and has been extensively and successfully used to measure diverse RNA–small-molecule interactions.[19,28−31] Indeed, ITC measurements are often taken to be a gold standard for characterizing binding interactions. However, ITC is low-throughput and consumptive of material, often requiring milligrams of RNA for a given program. SPR can be used to measure both the kinetics and thermodynamics of biomolecular binding events.[32] In an SPR experiment, one binding partner (termed the target here) is immobilized on a chemically functionalized gold surface, and the other binding partner (the analyte) is flowed across the surface in solution. Binding interactions cause a change in the refractive index near the surface, detected optically as an SPR response, generally expressed in response units (RU) (Figure 1).[32] SPR directly monitors small-molecule binding to the target RNA and, as a microfluidic platform, uses RNA and ligand material efficiently. SPR is scalable to moderately high-throughput workflows and has been broadly applied to diverse binding interactions, from large biomolecules[33] to low-molecular-weight fragment compounds.[34]

SPR experiments, using current-generation high sensitivity biosensors, are performed in a reference subtraction mode because injection of the analyte into the flow cell changes the refractive index of the solution and generates a binding-

Received: March 25, 2022
Revised: May 26, 2022
Published: July 8, 2022

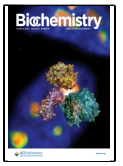

https://doi.org/10.1021/acs.biochem.2c00177
Biochemistry 2022, 61, 1625−1632

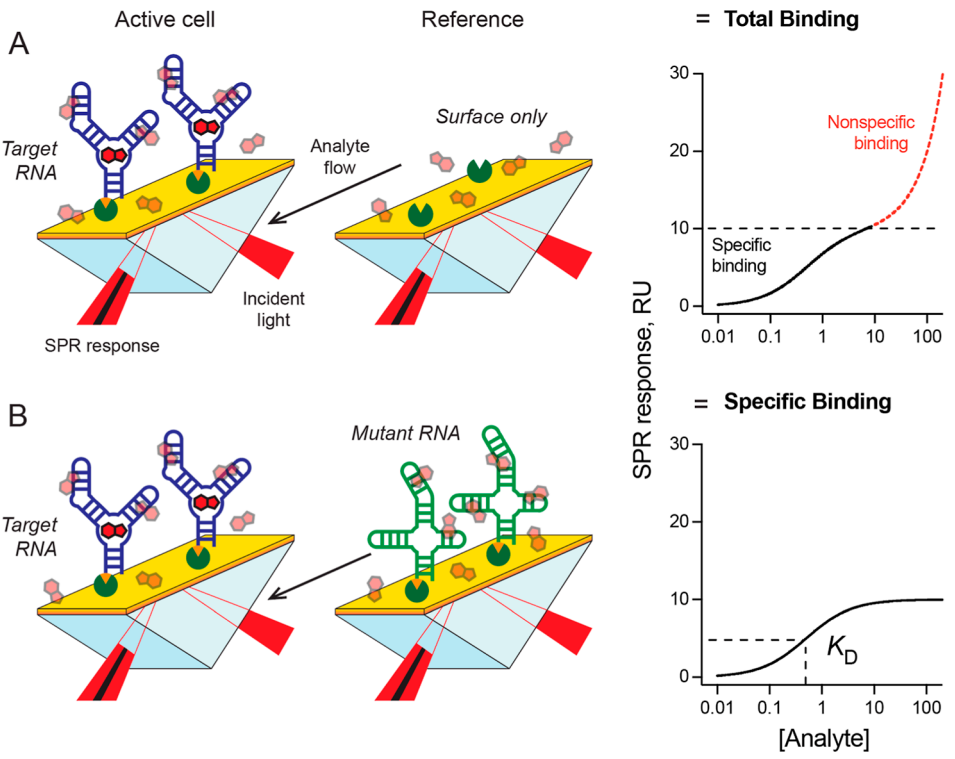

Figure 1. Overview of reference subtraction in an SPR experiment. (A) Referencing to a blank flow cell controls for bulk refractive index changes and allows quantification of the total surface-binding signal. (B) Use of a nonbinding RNA in the reference flow cell allows additional subtraction of the signal due to nonspecific analyte−macromolecule binding.

independent bulk response. To detect the target-specific binding response, the signal from a no-target reference flow cell is subtracted.[35] The reference flow cell is typically an empty cell, free of immobilized target (Figure 1A). Alternatively, a control molecule can be immobilized in the reference flow cell to better match experimental conditions between the active and reference flow cells. This latter strategy has been used in small-molecule fragment screens against protein targets to increase confidence that an experiment measures specific binding events.[34] We have found that nonspecific binding of candidate ligands to RNA, in part mediated by electrostatic interactions, often convolutes analysis of RNA-binding ligands by SPR, especially for weak binders.

Here, we explore reference subtraction as a strategy for measuring specific RNA−small-molecule interactions by SPR. We used a mutant or noncognate RNA, monitored in parallel to the target RNA, to control for the bulk sensor response and to enforce target specificity (Figure 1B). By analyzing well-characterized RNA−ligand pairs, spanning a wide range of binding affinities, we demonstrate that this experimental strategy yields dissociation constants that agree with those measured by other methods, including ITC. We provide guidelines for using SPR to examine RNA−small-molecule binding with the hope that this approach will broadly facilitate future efforts to target structured RNAs with small molecules.

MATERIALS AND METHODS

SPR Instrumentation and Running Buffers. SPR experiments were performed on a Biacore 8K SPR instrument (GE Healthcare Life Sciences). The flow cell was maintained at 25 °C. The running buffer was designed to mimic physiological-like chelated-Mg^{2+} conditions that increase RNA stability and function;[36] buffer consisted of 10 mM HEPES, pH 7.4, 150 mM NaCl, 13.3 mM $MgCl_2$, 96 mM glutamic acid, 0.05% TWEEN-20, and 1% DMSO. For the salt concentration dependence analysis (Figure S1), a modified running buffer was used (10 mM HEPES, pH 7.4, 2 mM $MgCl_2$, 0.05% TWEEN-20, and 1% DMSO, with 150 or 1000 mM NaCl). All solutions were prepared under RNase-free conditions with Milli-Q filtered water and sterile filtered through 0.2 μm filters (Thermo Scientific) before use.

RNA Preparation and Immobilization. 5′-Biotinylated RNAs were purchased from either Horizon Discovery or Integrated DNA Technologies and used without further purification. Prior to immobilization, RNAs were diluted to 1 μM in nuclease-free water, heated to 95 °C for 2 min, and then snap cooled on ice for 2 min. RNAs were then diluted to 500 nM with an equal volume of 2× running buffer and folded for 30 min at 37 °C before cooling to room temperature. RNA immobilization was carried out on streptavidin-functionalized sensor chips (Series S Sensor Chip SA, Cytiva). Immobilization involved a series of three injections of 1.0 M NaCl, 50 mM NaOH at a flow rate of 10 μL/min for 1 min to prepare the chip surface, followed by an injection of the RNA at 500 nM in running buffer, injected at a flow rate of 5 μL/min for 3−12 min depending on the desired immobilization level. Immobilization rates vary as a function of RNA size, concentration, biotinylation efficiency, and flow rate. Immobilization levels can be predictably fine-tuned by adjusting the contact time in the flow cell. Generally, immobilization levels of 2000−3000 RU were achieved and proved sufficient for small-molecule binding analysis. Following immobilization, buffer lines (excluding the flow cell) were washed with 1.0 M NaCl, 50 mM NaOH, and 50% isopropanol. Immobilized RNAs remained stable on the sensor chips over several days, although

https://doi.org/10.1021/acs.biochem.2c00177
Biochemistry 2022, 61, 1625−1632

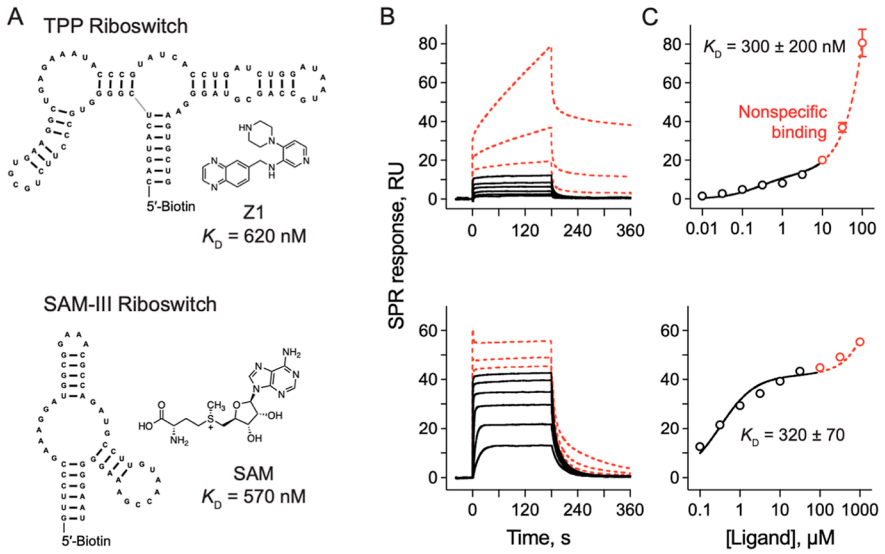

Figure 2. Small molecules bind RNA in both specific and nonspecific modes. (A) Secondary structures of the TPP and SAM-III riboswitch RNAs and their ligands **Z1** and SAM, respectively. (B) SPR sensorgrams and (C) binding curves for each small-molecule analyte. Sensorgrams and regions of the fits indicative of nonspecific binding are emphasized in red.

signal-to-noise ratios gradually decreased over time, as expected given the chemical lability of RNA at ambient temperature.

Preparation of Small-Molecule Analytes. In general, compounds were dissolved in DMSO at 1.0 M or 100 mM, then diluted 100-fold into a running buffer without DMSO, yielding a final DMSO concentration of 1%. Highly water-soluble compounds were dissolved directly in running buffer (1% DMSO) before dilution. After verifying solubility, analytes were serially diluted in running buffer in half-log (3.16-fold) increments to afford the final concentration series for analysis. Typically, nine concentrations covering a 10,000-fold concentration range yielded convincing binding data and made efficient use of a single 96-well plate. Solutions of small-molecule analytes were plated in 96-well U-bottom polypropylene plates (Greiner) and covered with microplate foils (Cytiva) prior to injection (to prevent evaporation).

Data Collection and Analysis. SPR analysis of compounds followed a multi-cycle affinity workflow: three running buffer injections (2 min at 30 μL/min) were performed to condition the chip surface. Subsequently, compounds were injected in a series of 10 injections (3 min analyte association, followed by 4 min dissociation, at 30 μL/min), starting with the no-analyte control, then increasing by analyte concentration (this scheme reduces carryover artifacts from high analyte concentrations). Each analyte injection sensorgram was double-reference subtracted: First, the signal from the reference flow cell (containing bare streptavidin or noncognate RNA) was subtracted to remove bulk solution contributions and nonspecific binding from the SPR signal. Second, the no-analyte injection signal was subtracted from all subsequent analyte injection sensorgrams to improve the baseline stability.[35] The steady-state SPR response for each injection was recorded as a 5 s average, beginning 10 s before the end of the association phase. All sensorgrams were examined qualitatively to confirm steady-state binding and full dissociation, consistent with established guidelines.[37]

Measuring Affinities for Tight-Binding Ligands. Thiamine pyrophosphate (TPP), the native ligand of the TPP riboswitch and the highest-affinity compound studied, exhibited slow dissociation rates such that the analyte was retained on the immobilized target during the standard dissociation period, reducing the response amplitude of subsequent injections. To measure binding of the TPP ligand, we therefore accelerated TPP dissociation by performing injections with no-Mg^{2+} running buffer (10 mM HEPES, pH 7.4, 150 mM NaCl, 96 mM glutamic acid, 0.05% TWEEN-20, and 1% DMSO; 2 min at 30 μL/min) between each analyte injection (Figure S2).

Fitting of SPR Data to Obtain K_D. Steady-state SPR responses for each analyte injection as a function of analyte concentration were fit (GraphPad Prism) by least-squares regression to a total binding model

$$R = R_{max}\frac{[\text{Analyte}]}{(K_D + [\text{Analyte}])} + NS\,[\text{Analyte}] \quad (1)$$

where R is the observed SPR response in RU, R_{max} is the maximal SPR response at the saturating analyte, K_D is the binding dissociation constant in units of molar concentrations, NS is the slope describing linear and nonspecific binding, and [Analyte] is the small-molecule analyte concentration in the mobile phase. If NS is zero, this equation is equivalent to that for one-site binding. For most of this work (Figures 2−4, and S1), all parameters in eq 1 were unrestricted. For global ligand analysis (Figure 5 and S2, Table S1 and S2), the nonspecific binding coefficient NS was fixed at 0. All binding titrations were performed in triplicate. Best-fit values for K_D and NS are reported ±standard error, based on the symmetric confidence interval from global data fitting.

Estimating R_{max} for Nonsaturating Ligands. In cases where weak binders are unable to fully saturate the immobilized target, binding curves can be approximated by estimating R_{max} as[37,38]

$$R_{max} = N\frac{MW_{Analyte}}{MW_{Target}}R_i \quad (2)$$

where R_{max} is the maximal SPR response for single-site saturated binding, $MW_{Analyte}$ and MW_{Target} are the molecular weights of the free and immobilized binding partners,

https://doi.org/10.1021/acs.biochem.2c00177
Biochemistry 2022, 61, 1625−1632

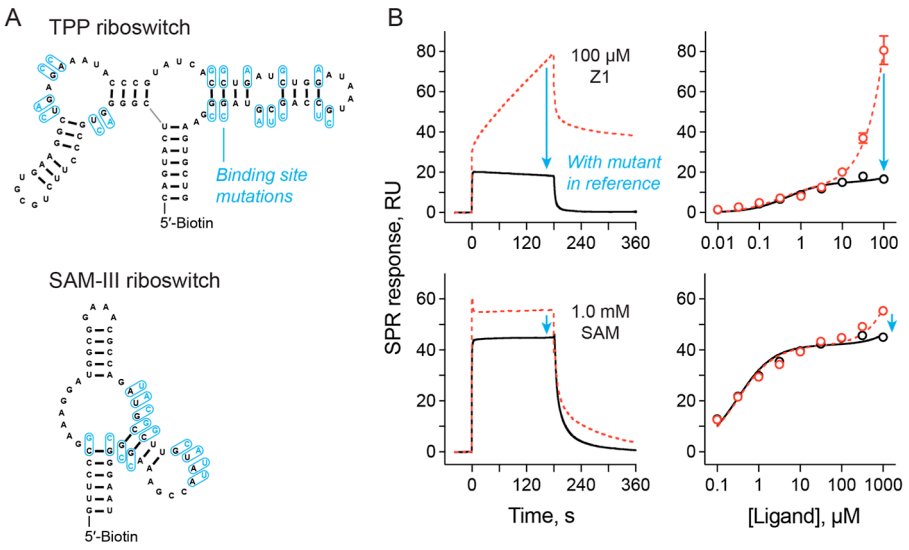

C

Target RNA	Ligand	With mutant in reference	K_D (nM)	*NS* (RU/nM)
TPP riboswitch	Z1	–	300 ± 200	690 ± 30
		+	500 ± 100	20 ± 20
SAM-III riboswitch	SAM	–	320 ± 70	15 ± 3
		+	310 ± 60	4 ± 3

Figure 3. Referencing to mutant RNA subtracts nonspecific binding. (A) Mutations (blue) introduced in the binding sites for the TPP and SAM-III riboswitch RNAs to disrupt specific binding. (B) Representative SPR sensorgrams (left) and binding curves (right) with and without a binding site mutant in the reference channel. Arrows emphasize the effect of incorporating the reference RNA. (C) Values for K_D and *NS* (eq 1) as a function of the reference channel.

respectively, R_i is the SPR response observed during target immobilization, and N is a heuristic parameter, representing the fractional response. The following features can affect the eq 2 relationship and N: (i) analytes vary in their contribution to the SPR response: nucleic acids exhibit a SPR response that is about 30% greater by mass concentration than that for proteins,[39] and SPR responses of small molecules of a given mass vary by as much as two-fold.[40] (ii) The R_{max} relationship assumes that all immobilized RNA is intact, properly folded, and available for ligand binding. (iii) Conformational changes in nucleic acids can affect an SPR binding response.[41,42]

RESULTS

Specific and Semispecific Ligand Binding to RNA. To evaluate SPR as a method for measuring RNA–small-molecule-binding affinities, we initially focused on two RNA–ligand pairs: a synthetic ligand developed in our laboratory that binds to the *Escherichia coli* TPP riboswitch,[31] termed **Z1**, and *S*-adenosyl methionine (SAM), the cognate ligand for a crystallography-optimized construct of the *Enterococcus faecalis* SAM-III (S_{MK} box) riboswitch.[22] These compounds bind to their target riboswitches with sub-μM affinity at a single site. Each RNA construct consisted of only the riboswitch aptamer domain to avoid complications arising from RNA structural rearrangements (Figure 2A). The riboswitch RNAs were immobilized in SPR flow cells to ~2600 RU, and small-molecule analytes were injected. For each analyte injection, the signal from a no-target reference flow cell was subtracted to remove the binding-independent bulk response. Concentration-dependent SPR responses were observed for both RNA–small-molecule pairs (Figure 2B). However, evidence for nonspecific binding is visible in the **Z1** sensorgrams by a transition from rectangular profiles at low ligand concentrations, indicative of rapid steady-state binding kinetics, to upwardly sloping profiles at high ligand concentrations, indicative of slow, non-steady-state binding (Figure 2B, top). For the SAM ligand, the amplitude of the sensorgrams initially plateaus but then increases at high ligand concentrations, also suggestive of nonspecific binding (Figure 2B, bottom). The resulting data then fit poorly to a single-site binding model in both cases but yield a notably better fit using a total binding model that includes a linear, nonspecific binding term (Figure 2C, eq 1).

Given the negatively charged phosphoribose backbone of RNA, we suspected that one predominant contributor to nonspecific binding was electrostatic attraction to the positively charged small molecules. Increasing the concentration of Na^+ ions in the running buffer reduced, but did not eliminate, nonspecific binding, suggesting that high ionic strength buffer partially, but incompletely, shields electrostatic interactions (Figure S1). Nonspecific binding has been observed previously in SPR experiments that measured interactions between RNA and small molecules, particularly with cationic aminoglycoside antibiotics.[26,43] In our experience, nonspecific binding is most pronounced for positively charged ligands but can occur with broad classes of ligands. For high-affinity binders, specific and nonspecific binding regimes are often sufficiently distinct to be resolved by data fitting to eq 1. However, to accurately measure weak binding affinities, including those of fragment ligands, a superior strategy would

https://doi.org/10.1021/acs.biochem.2c00177
Biochemistry 2022, 61, 1625–1632

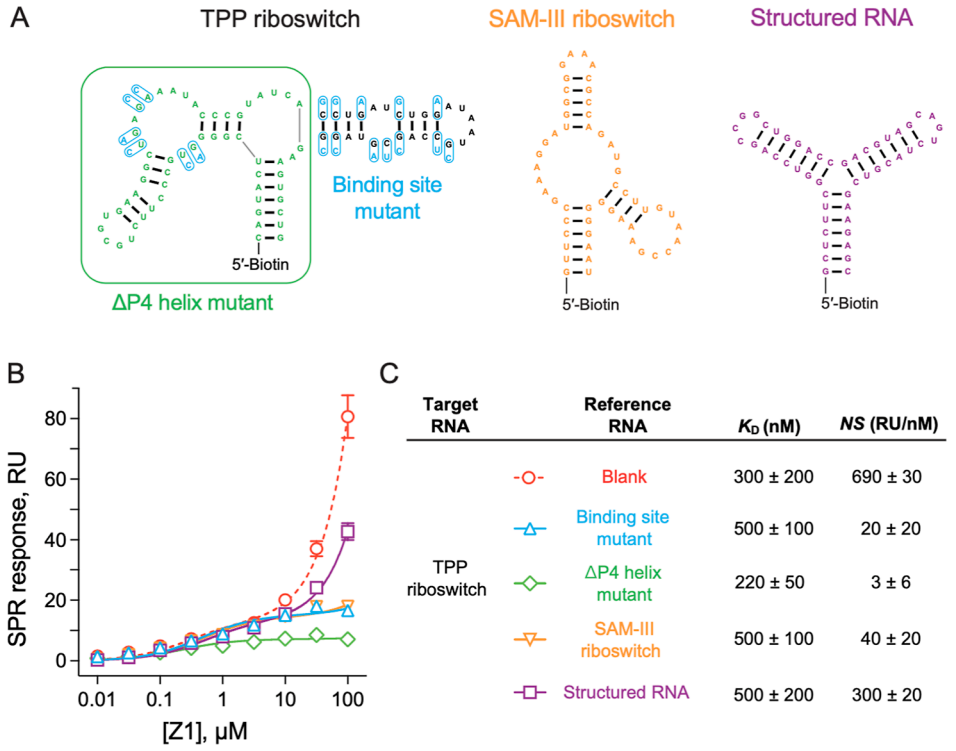

Figure 4. Impact of reference RNA choice on nonspecific binding subtraction. (A) Secondary structures of RNAs used for reference subtraction. Note that the binding site mutant requires high levels of prior structural knowledge, whereas the ΔP4 mutant, SAM-III riboswitch, and structured RNA controls do not. (B) SPR responses for **Z1** binding to the TPP riboswitch, using subtraction with different reference RNAs. (C) Values of K_D and *NS* (eq 1) for **Z1** binding the TPP riboswitch as a function of reference RNA.

involve subtracting the nonspecific binding signal via an improved experiment.

Mutant Referencing Subtracts Nonspecific Binding. SPR signals are measured by comparison to a reference channel, and we reasoned that a noncognate RNA immobilized in the reference flow cell would allow for subtraction of signals due to nonspecific binding of small-molecule analytes (Figure 1B). Based on the crystal structures of the TPP and SAM-III riboswitch RNAs,[22,44] we designed RNA constructs with targeted mutations in each ligand-binding site to disrupt specific target engagement (Figure 3A). When SPR experiments were performed with the native sequence and mutant RNAs in the active and reference flow cells, respectively, the SPR responses for **Z1** and SAM were attenuated at high analyte concentrations. For example, in the case of **Z1**, the sensorgram shape was greatly improved at high analyte concentrations, with profiles indicative of fast binding kinetics and one-site interaction typical of small molecules (Figure 3B, top). When data from each concentration series were fit to eq 1, the slopes characterizing nonspecific binding were significantly reduced for experiments performed with reference RNA subtraction (Figure 3C). Thus, using a non-binding RNA in the reference channel, SPR responses for two RNA−small-molecule pairs were characterized by simple single-site binding, and nonspecific binding effects were removed.

Analysis of Reference Mutant Specificity. The reference RNA mutants used for this first set of experiments were "high information" constructs, designed based on known binding sites, as visualized in high-resolution structures. To be broadly useful, nonspecific subtraction should be implemented with a generic, "low information" reference RNA. We analyzed **Z1** binding to the TPP riboswitch using alternative RNAs in the reference flow cell, including the original binding site mutant, a mutant that deletes the P4 helix (ΔP4), the SAM-III riboswitch RNA, and a structured RNA of arbitrary sequence, corresponding to decreasing levels of binding site information (Figure 4A).

Encouragingly, referencing to the non-cognate SAM-III riboswitch achieved the same level of nonspecific subtraction as the targeted binding site mutant, and measured K_D values were virtually the same for both reference RNAs (Figure 4B). Referencing to the ΔP4 helix mutant eliminated nonspecific binding but also reduced overall signal amplitude. The ΔP4 helix mutant contains an intact portion of the TPP riboswitch ligand-binding site, and **Z1** may show some semispecific binding to both target and reference RNAs, resulting in over-subtraction. Use of the de novo-designed structured RNA yielded notable, but modest, improvement over the blank reference experiment but did not fully reduce non-specific binding at high concentrations of **Z1**. This RNA likely was too structured, containing too few single-stranded elements, to adequately capture nonspecific binding to **Z1**.

Validation on Known RNA−Ligand Pairs. To further examine reference-subtracted SPR, we examined a set of compounds known to bind each of our RNA targets (Table S1). For the TPP riboswitch, the compounds examined bind with nanomolar to millimolar equilibrium dissociation constants, as measured by ITC.[31,45] We also examined TPP and its derivative thiamine, for which the binding affinities have been measured by numerous biophysical methods.[7,14,19,46] For the SAM-III riboswitch RNA, we examined SAM and *S*-adenosyl homocysteine (SAH). SAM binds with sub-μM affinity, as measured by ITC, size exclusion filtration, and fluorescence quenching of a 2-aminopurine-substituted

https://doi.org/10.1021/acs.biochem.2c00177
Biochemistry 2022, 61, 1625−1632

RNA.[22,47] Using the reported 2-aminopurine fluorescence assay, we measured a K_D for SAH of 80 μM. Collectively, these compounds have low molecular masses, span a broad range of binding affinities, and are representative of compounds that might be identified or explored in RNA ligand analysis or hit identification projects.

We evaluated the binding affinities of these compounds by SPR, referencing to the binding-site mutants designed to serve as controls for each riboswitch construct. The resulting SPR responses were fit to a single-site binding equation with the nonspecific binding term set to zero (Figure S2). Measured SPR dissociation constants show excellent correlation with reported affinities measured by ITC and other methods (Figure 5, Table S1). Interestingly, we find that the best-fit

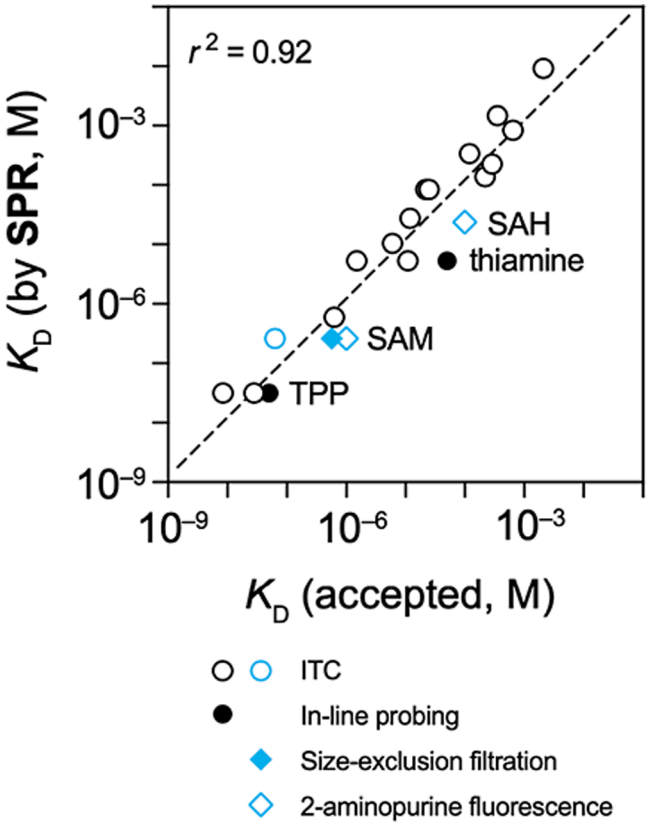

Figure 5. Correlation between dissociation constants determined by SPR with those obtained using other methods. K_D values for ligands of the TPP (black) and SAM-III (blue) riboswitch RNAs measured by SPR, using a binding-site mutant RNA for reference subtraction (Figure 3), plotted vs values determined by ITC and other methods (Table S1). Correlation analysis is based on values for log(K_D).

experimental values for R_{max} average 0.6-fold of the value predicted based on simple consideration of relative mass (eq 2, Table S2). This observation provides a guideline for interpreting future SPR measurements of RNA–ligand binding. Broadly, SPR with reference subtraction yields accurate equilibrium dissociation constants for RNA-binding ligands across a wide range of affinities.

DISCUSSION

We examined the ability of SPR to measure RNA–ligand-binding affinities, spanning over five orders of magnitude. We demonstrate that incorporating a suitable reference RNA subtracts nonspecific binding, which appears widespread across the RNA ligands studied here. For the ligands studied here, electrostatic interactions appear to be the predominant mechanism of nonspecific binding. Reference subtraction will likely similarly control for nonspecific binding by other mechanisms, including nonspecific stacking and intercalation. Use of a reference RNA additionally equalizes macromolecular crowding near the active and reference surfaces, which can influence SPR responses at high analyte concentrations. Reference RNAs can be designed to enforce varying levels of specificity, from high-information constructs that select for binding-site-specific interactions, to noncognate reference RNAs that tolerate a greater variety of binding modes. For investigating novel binding interactions, it may be advantageous to work with multiple reference RNAs, to test for the possibility of under- and over-subtraction. Reference subtraction is most effective when the target and reference RNAs are immobilized to similar RU values, corresponding to equal loading of RNA (by mass) on each surface. In our view, SPR with reference subtraction becomes a first-choice strategy for measuring affinities of RNA–ligand interactions.

SPR offers multiple advantages for measuring RNA–ligand binding. Experiments are performed with a few micrograms of biotinylated RNA. Small RNAs can be produced synthetically, while larger RNAs can be produced by in vitro transcription and then end-labeled with biotin by chemical or enzymatic methods.[48−50] Structurally complex RNAs, which are likely to feature binding pockets that make them attractive targets for selective small-molecule probes,[6] are readily examined. We consistently observe that SPR can successfully measure binding affinities of low-molecular weight, weakly binding (fragment) ligands. Fragment screens have been widely adopted,[51] and growing evidence supports that fragment-based screening is well-suited for targeting RNA.[31,52,53] The orthogonal methods outlined in the introduction yield valuable information about RNA–ligand binding, including thermodynamics (ITC); RNA structure, ligand engagement, and conformational rearrangements (chemical probing); and atomic-resolution binding modes (NMR). SPR surpasses these methods in throughput and efficient use of material. The SPR strategy described here does not meet the throughput demands for first-round screening, but is a powerful tool for validating potential ligands and for efficiently guiding development of high-affinity analogues.

Two limitations arise from our work that are specific to RNA–small-molecule SPR. First, despite careful experimentation, we observe that analyte binding responses slowly diminish after RNA immobilization, likely due to a combination of physical RNA degradation and formation of non-binding RNA conformations, reducing analyte binding responses. The biotin–streptavidin immobilization used here is essentially irreversible, and thus signal degradation renders the target-immobilized sensor chip surface unusable after several days, limiting assay throughput. Second, we observe that larger RNAs immobilize more slowly and to a lower maximum response than smaller RNAs, possibly due to limited diffusion into the dextran matrix of the sensor chip surface. This lower mass of immobilized RNA, compounded by the higher-molecular weight of such targets, means that ligand-binding responses for large RNAs can be low. Based on our experience with RNA immobilization levels and maximal ligand responses, we estimate that RNAs shorter than 200 nucleotides will be consistently good candidates for measurements of ligand

https://doi.org/10.1021/acs.biochem.2c00177
Biochemistry 2022, 61, 1625−1632

binding by SPR; we have successfully applied SPR to RNAs of ∼300 nucleotides in favorable cases. For RNAs longer than 300 nucleotides (∼100 kDa), the maximal expected SPR response for a small-molecule ligand falls below 1 RU, comparable to instrument background noise.

In sum, SPR is highly sensitive, moderate throughput, and material efficient, making it an attractive platform for measuring RNA−ligand binding. When implemented with reference subtraction, SPR reliably discriminates specific and nonspecific binding, a principal concern of ligand development programs. We anticipate that, with the examples and guidelines described here, SPR merits widespread consideration as a first-choice method for measuring RNA−ligand-binding affinities and will accelerate discovery of RNA-targeting ligands, and ultimately, entry into therapeutics.

■ ASSOCIATED CONTENT

Supporting Information

The Supporting Information is available free of charge at https://pubs.acs.org/doi/10.1021/acs.biochem.2c00177.

Two tables and two figures describing comparison of SPR versus accepted dissociation constants for compounds that bind to the TPP and SAM-III riboswitch RNAs; predicted versus best fit values for R_{max}; effects of high Na^+ concentrations on nonspecific RNA−ligand interactions; and SPR sensorgrams and binding curves for compounds that bind the TPP and SAM-III riboswitch RNAs (PDF)

■ AUTHOR INFORMATION

Corresponding Author

Kevin M. Weeks − *Department of Chemistry, University of North Carolina, Chapel Hill, North Carolina 27599-3290, United States;* orcid.org/0000-0002-6748-9985; Email: weeks@unc.edu

Author

J. Winston Arney − *Department of Chemistry, University of North Carolina, Chapel Hill, North Carolina 27599-3290, United States*

Complete contact information is available at: https://pubs.acs.org/10.1021/acs.biochem.2c00177

Notes

The authors declare the following competing financial interest(s): K.M.W. is an advisor to and holds equity in Ribometrix.

■ ACKNOWLEDGMENTS

This work was supported by the US National Institutes of Health (R01 HL111527 to K.M.W. and Alain Laederach and R35 GM122532 to K.M.W.). SPR experiments were performed in the UNC Macromolecular Interactions Facility (supported by P30 CA016086). The authors thank Jarett Story for performing SAM riboswitch binding experiments and Dr. Ashutosh Tripathy for training on and assistance with SPR experiments.

■ REFERENCES

(1) Breaker, R. R. Prospects for Riboswitch Discovery and Analysis. *Mol. Cell* **2011**, *43*, 867−879.

(2) Wilson, D. N. Ribosome-targeting antibiotics and mechanisms of bacterial resistance. *Nat. Rev. Microbiol.* **2014**, *12*, 35−48.

(3) Dunn, M. R.; Jimenez, R. M.; Chaput, J. C. Analysis of aptamer discovery and technology. *Nat. Rev. Chem.* **2017**, *1*, 0076.

(4) Berens, C.; Groher, F.; Suess, B. RNA aptamers as genetic control devices: The potential of riboswitches as synthetic elements for regulating gene expression. *Biotechnol. J.* **2015**, *10*, 246−257.

(5) Connelly, C. M.; Moon, M. H.; Schneekloth, J. S. The Emerging Role of RNA as a Therapeutic Target for Small Molecules. *Cell Chem. Biol.* **2016**, *23*, 1077−1090.

(6) Warner, K. D.; Hajdin, C. E.; Weeks, K. M. Principles for targeting RNA with drug-like small molecules. *Nat. Rev. Drug Discovery* **2018**, *17*, 547−558.

(7) Winkler, W.; Nahvi, A.; Breaker, R. R. Thiamine derivatives bind messenger RNAs directly to regulate bacterial gene expression. *Nature* **2002**, *419*, 952−956.

(8) Regulski, E. E.; Breaker, R. R. In-line probing analysis of riboswitches. *Methods Mol. Biol.* **2008**, *419*, 53−67.

(9) Douthwaite, S. Interaction of the antibiotics clindamycin and lincomycin with Escherichia coli 23S ribosomal RNA. *Nucleic Acids Res.* **1992**, *20*, 4717−4720.

(10) Hansen, L. H.; Mauvais, P.; Douthwaite, S. The macrolide-ketolide antibiotic binding site is formed by structures in domains II and V of 23S ribosomal RNA. *Mol. Microbiol.* **1999**, *31*, 623−631.

(11) Wang, B.; Wilkinson, K. A.; Weeks, K. M. Complex ligand-induced conformational changes in $tRNA^{Asp}$ revealed by single-nucleotide resolution SHAPE chemistry. *Biochemistry* **2008**, *47*, 3454−3461.

(12) Sztuba-Solinska, J.; Shenoy, S. R.; Gareiss, P.; Krumpe, L. R. H.; Le Grice, S. F. J.; O'Keefe, B. R.; Schneekloth, J. S. Identification of biologically active, HIV TAR RNA-binding small molecules using small molecule microarrays. *J. Am. Chem. Soc.* **2014**, *136*, 8402−8410.

(13) Kulshina, N.; Edwards, T. E.; Ferré-D'Amaré, A. R. Thermodynamic analysis of ligand binding and ligand binding-induced tertiary structure formation by the thiamine pyrophosphate riboswitch. *RNA* **2010**, *16*, 186−196.

(14) Yamauchi, T.; Miyoshi, D.; Kubodera, T.; Nishimura, A.; Nakai, S.; Sugimoto, N. Roles of Mg^{2+} in TPP-dependent riboswitch. *FEBS Lett.* **2005**, *579*, 2583−2588.

(15) Smith, A. M.; Fuchs, R. T.; Grundy, F. J.; Henkin, T. M. The SAM-responsive S_{MK} box is a reversible riboswitch. *Mol. Microbiol.* **2010**, *78*, 1393−1402.

(16) Hall, K. B. 2-aminopurine as a probe of RNA conformational transitions. *Methods Enzymol.* **2009**, *469*, 269−285.

(17) Wicks, S. L.; Hargrove, A. E. Fluorescent indicator displacement assays to identify and characterize small molecule interactions with RNA. *Methods* **2019**, *167*, 3−14.

(18) Mayer, M.; James, T. L. Detecting ligand binding to a small RNA target via saturation transfer difference NMR experiments in D_2O and H_2O. *J. Am. Chem. Soc.* **2002**, *124*, 13376−13377.

(19) Cressina, E.; Chen, L.; Abell, C.; Leeper, F. J.; Smith, A. G. Fragment screening against the thiamine pyrophosphate riboswitch thiM. *Chem. Sci.* **2011**, *2*, 157−165.

(20) Moon, M. H.; Hilimire, T. A.; Sanders, A. M.; Schneekloth, J. S. Measuring RNA-Ligand Interactions with Microscale Thermophoresis. *Biochemistry* **2018**, *57*, 4638−4643.

(21) Reiss, C. W.; Xiong, Y.; Strobel, S. A. Structural Basis for Ligand Binding to the Guanidine-I Riboswitch. *Structure* **2017**, *25*, 195−202.

(22) Lu, C.; Smith, A. M.; Fuchs, R. T.; Ding, F.; Rajashankar, K.; Henkin, T. M.; Ke, A. Crystal structures of the SAM-III/SMK riboswitch reveal the SAM-dependent translation inhibition mechanism. *Nat. Struct. Mol. Biol.* **2008**, *15*, 1076−1083.

(23) Salim, N. N.; Feig, A. L. Isothermal titration calorimetry of RNA. *Methods* **2009**, *47*, 198−205.

(24) Gilbert, S. D.; Batey, R. T. Monitoring RNA−ligand interactions using isothermal titration calorimetry. *Methods Mol. Biol.* **2009**, *540*, 97−114.

(25) Nguyen, B.; Tanious, F. A.; Wilson, W. D. Biosensor-surface plasmon resonance: Quantitative analysis of small molecule-nucleic acid interactions. *Methods* **2007**, *42*, 150−161.
(26) Hendrix, M.; Priestley, E. S.; Joyce, G. F.; Wong, C.-H. Direct observation of aminoglycoside−RNA interactions by surface plasmon resonance. *J. Am. Chem. Soc.* **1997**, *119*, 3641−3648.
(27) Chaires, J. B. Calorimetry and thermodynamics in drug design. *Annu. Rev. Biophys.* **2008**, *37*, 135−151.
(28) Batey, R. T.; Gilbert, S. D.; Montange, R. K. Structure of a natural guanine-responsive riboswitch complexed with the metabolite hypoxanthine. *Nature* **2004**, *432*, 411−415.
(29) Baird, N. J.; Ferré-D'Amaré, A. R. Idiosyncratically tuned switching behavior of riboswitch aptamer domains revealed by comparative small-angle X-ray scattering analysis. *RNA* **2010**, *16*, 598−609.
(30) Tran, B.; Pichling, P.; Tenney, L.; Connelly, C. M.; Moon, M. H.; Ferré-D'Amaré, A. R.; Schneekloth, J. S.; Jones, C. P. Parallel Discovery Strategies Provide a Basis for Riboswitch Ligand Design. *Cell Chem. Biol.* **2020**, *27*, 1241−1249.e4.
(31) Zeller, M. J.; Favorov, O.; Li, K.; Nuthanakanti, A.; Hussein, D.; Michaud, A.; Lafontaine, D. A.; Busan, S.; Serganov, A.; Aubé, J.; Weeks, K. M. SHAPE-enabled fragment-based ligand discovery for RNA. *Proc. Natl. Acad. Sci. U.S.A.* **2022**, *119*, e2122660119.
(32) Schuck, P. Use of surface plasmon resonance to probe the equilibrium and dynamic aspects of interactions between biological macromolecules. *Annu. Rev. Biophys. Biomol. Struct.* **1997**, *26*, 541−566.
(33) Malmqvist, M. Surface plasmon resonance for detection and measurement of antibody-antigen affinity and kinetics. *Curr. Opin. Immunol.* **1993**, *5*, 282−286.
(34) Navratilova, I.; Hopkins, A. L. Fragment screening by surface plasmon resonance. *ACS Med. Chem. Lett.* **2010**, *1*, 44−48.
(35) Myszka, D. G. Improving biosensor analysis. *J. Mol. Recognit.* **1999**, *12*, 279−284.
(36) Yamagami, R.; Bingaman, J. L.; Frankel, E. A.; Bevilacqua, P. C. Cellular conditions of weakly chelated magnesium ions strongly promote RNA stability and catalysis. *Nat. Commun.* **2018**, *9*, 2149.
(37) Giannetti, A. M. From experimental design to validated hits: A comprehensive walk-through of fragment lead identification using surface plasmon resonance. *Methods Enzymol.* **2011**, *493*, 169−218.
(38) Vo, T.; Paul, A.; Kumar, A.; Boykin, D. W.; Wilson, W. D. Biosensor-surface plasmon resonance: A strategy to help establish a new generation RNA-specific small molecules. *Methods* **2019**, *167*, 15−27.
(39) Buckle, M.; Williams, R. M.; Negroni, M.; Buc, H. Real time measurements of elongation by a reverse transcriptase using surface plasmon resonance. *Proc. Natl. Acad. Sci. U.S.A.* **1996**, *93*, 889−894.
(40) Davis, T. M.; Wilson, W. D. Determination of the refractive index increments of small molecules for correction of surface plasmon resonance data. *Anal. Biochem.* **2000**, *284*, 348−353.
(41) Dejeu, J.; Bonnet, H.; Spinelli, N.; Defrancq, E.; Coche-Guérente, L.; Van Der Heyden, A.; Labbé, P. Impact of Conformational Transitions on SPR Signals - Theoretical Treatment and Application in Small Analytes/Aptamer Recognition. *J. Phys. Chem. C* **2018**, *122*, 21521−21530.
(42) Bonnet, H.; Coche-Guérente, L.; Defrancq, E.; Spinelli, N.; Van der Heyden, A.; Dejeu, J. Negative SPR signals during low molecular weight analyte recognition. *Anal. Chem.* **2021**, *93*, 4134−4140.
(43) Davis, T. M.; David Wilson, W. Surface plasmon resonance biosensor analysis of RNA-small molecule interactions. *Methods Enzymol.* **2001**, *340*, 22−51.
(44) Serganov, A.; Polonskaia, A.; Phan, A. T.; Breaker, R. R.; Patel, D. J. Structural basis for gene regulation by a thiamine pyrophosphate-sensing riboswitch. *Nature* **2006**, *441*, 1167−1171.
(45) Zeller, M. J.; Nuthanakanti, A.; Li, K.; Aubé, J.; Serganov, A.; Weeks, K. M. Subsite Ligand Recognition and Cooperativity in the TPP Riboswitch: Implications for Fragment-Linking in RNA Ligand Discovery. *ACS Chem. Biol.* **2022**, *17*, 438−448.
(46) Sudarsan, N.; Cohen-Chalamish, S.; Nakamura, S.; Emilsson, G. M.; Breaker, R. R. Thiamine pyrophosphate riboswitches are targets for the antimicrobial compound pyrithiamine. *Chem. Biol.* **2005**, *12*, 1325−1335.
(47) Wilson, R. C.; Smith, A. M.; Fuchs, R. T.; Kleckner, I. R.; Henkin, T. M.; Foster, M. P. Tuning riboswitch regulation through conformational selection. *J. Mol. Biol.* **2011**, *405*, 926−938.
(48) Awwad, D. A.; Rahmouni, A. R.; Aboul-ela, F. Protocol for efficient fluorescence 3′ end-labeling of native noncoding RNA domains. *MethodsX* **2020**, *7*, 101148.
(49) Klöcker, N.; Weissenboeck, F. P.; Rentmeister, A. Covalent labeling of nucleic acids. *Chem. Soc. Rev.* **2020**, *49*, 8749−8773.
(50) Moritz, B.; Wahle, E. Simple methods for the 3' biotinylation of RNA. *RNA* **2014**, *20*, 421−427.
(51) Erlanson, D. A.; Fesik, S. W.; Hubbard, R. E.; Jahnke, W.; Jhoti, H. Twenty years on: The impact of fragments on drug discovery. *Nat. Rev. Drug Discovery* **2016**, *15*, 605−619.
(52) Lundquist, K. P.; Panchal, V.; Gotfredsen, C. H.; Brenk, R.; Clausen, M. H. Fragment-Based Drug Discovery for RNA Targets. *ChemMedChem* **2021**, *16*, 2588−2603.
(53) Sreeramulu, S.; Richter, C.; Berg, H.; Wirtz Martin, M. A.; Ceylan, B.; Matzel, T.; Adam, J.; Altincekic, N.; Azzaoui, K.; Bains, J. K.; Blommers, M. J. J.; Ferner, J.; Fürtig, B.; Göbel, M.; Grün, J. T.; Hengesbach, M.; Hohmann, K. F.; Hymon, D.; Knezic, B.; Martins, J. N.; Mertinkus, K. R.; Niesteruk, A.; Peter, S. A.; Pyper, D. J.; Qureshi, N. S.; Scheffer, U.; Schlundt, A.; Schnieders, R.; Stirnal, E.; Sudakov, A.; Tröster, A.; Vögele, J.; Wacker, A.; Weigand, J. E.; Wirmer-Bartoschek, J.; Wöhnert, J.; Schwalbe, H. Exploring the Druggability of Conserved RNA Regulatory Elements in the SARS-CoV-2 Genome. *Angew. Chem., Int. Ed.* **2021**, *60*, 19191−19200.

https://doi.org/10.1021/acs.biochem.2c00177
Biochemistry 2022, 61, 1625−1632